

Responsive Noise-Relaying Diffusion Policy: Responsive and Efficient Visuomotor Control

Zhuoqun Chen*
UC San Diego

zhc057@ucsd.edu

Xiu Yuan*
UC San Diego

x1yuan@ucsd.edu

Tongzhou Mu
UC San Diego

t3mu@ucsd.edu

Hao Su
UC San Diego

haosu@ucsd.edu

Abstract

Imitation learning is an efficient method for teaching robots a variety of tasks. Diffusion Policy, which uses a conditional denoising diffusion process to generate actions, has demonstrated superior performance, particularly in learning from multi-modal demonstrates. However, it relies on executing multiple actions to retain performance and prevent mode bouncing, which limits its responsiveness, as actions are not conditioned on the most recent observations. To address this, we introduce Responsive Noise-Relaying Diffusion Policy (RNR-DP), which maintains a noise-relaying buffer with progressively increasing noise levels and employs a sequential denoising mechanism that generates immediate, noise-free actions at the head of the sequence, while appending noisy actions at the tail. This ensures that actions are responsive and conditioned on the latest observations, while maintaining motion consistency through the noise-relaying buffer. This design enables the handling of tasks requiring responsive control, and accelerates action generation by reusing denoising steps. Experiments on response-sensitive tasks demonstrate that, compared to Diffusion Policy, ours achieves 18% improvement in success rate. Further evaluation on regular tasks demonstrates that RNR-DP also exceeds the best acceleration method by 6.9%, highlighting its computational efficiency advantage in scenarios where responsiveness is less critical.

1 Introduction

Imitation learning is a powerful approach for training robots to perform complex tasks, including grasping (Johns, 2021; Xie et al., 2020; Stepputtis et al., 2020), legged locomotion (Ratliff et al., 2007; Al-Hafez et al., 2023; Yang et al., 2023b), dexterous manipulation (Qin et al., 2022; Radosavovic et al., 2021), and mobile manipulation (Wong et al., 2022; Du et al., 2022). Advances in computer vision and natural language processing have led to increasingly sophisticated imitation learning frameworks, achieving impressive success across diverse tasks (Chen et al., 2021; Abramson, 1970; Florence et al., 2022; Shafullah et al., 2022). A notable breakthrough, Diffusion Policy (Chi et al., 2023), models robot action sequences through a conditional denoising diffusion process, setting new benchmarks over traditional imitation learning techniques. Consequently, Diffusion Policy has rapidly gained traction and is now widely adopted as a foundational framework in both research and real-world applications.

*These authors contributed equally to this work.

However, Diffusion Policy faces significant limitations. As shown in Chi et al. (2023), its performance heavily depends on having a relatively large action horizon, T_a , which corresponds to executing multiple actions in the environment. The policy widely achieves optimal performance at $T_a = 8$ but suffers substantial degradation when $T_a = 1$, where only a single action is executed per inference. We attribute this to the nature of modeling multi-modal data: each inference independently samples actions aligned with a specific mode. Consequently, a larger action horizon is essential to ensure a sequence of actions adheres to the same mode, maintaining consistency. Conversely, using $T_a = 1$ leads to severe mode bouncing, causing significant performance drops. However, employing a large action horizon (e.g., $T_a = 8$) also introduces drawbacks, as most actions are not conditioned on the latest observations, thereby reducing responsiveness and adaptability to environmental changes. Empirically, we observe that Diffusion Policy struggles particularly with tasks requiring responsive control, such as handling dynamic objects.

To address these issues, we propose the Responsive Noise-Relaying Diffusion Policy (RNR-DP). This approach fundamentally relies on a noise-relaying buffer that contains increasing noise levels and implements a sequential denoising mechanism. After each denoising step, conditioned on the most recent observations, the model executes an immediate noise-free action at the buffer’s head and appends fully noisy actions at the buffer’s tail. The noise-relaying buffer, combined with the sequential denoising mechanism, not only reuses denoising steps from previous outputs—allowing one denoising step to generate one action—but also ensures active control based on the most recent observations and prevents frequent mode bouncing, maintaining action consistency throughout the entire process. We name it **Responsive Noise-Relaying Diffusion Policy** because it employs a **noise-relaying buffer** at its core and has the ability to **respond quickly and actively to the environment**.

We evaluate our approach across a range of benchmarks, focusing on 9 tasks from three well-established datasets: ManiSkill2 (Gu et al., 2023), ManiSkill3 (Tao et al., 2024), and Adroit (Rajeswaran et al., 2017). Our primary evaluation targets 5 tasks involving dynamic object manipulation that demand responsive control. Empirical results show that RNR-DP significantly outperforms Diffusion Policy, delivering much more responsive control. Additionally, we extend our evaluation to tasks that do not require responsive control. The results indicate that, even on these simpler tasks, RNR-DP functions as a superior acceleration method compared to popular alternatives such as DDIM (Song et al., 2020) and Consistency Policy (Song et al., 2023; Prasad et al., 2024). Overall, our evaluations systematically demonstrate that RNR-DP provides both highly responsive and efficient control.

To summarize, our contributions are as follows:

- We identify a key limitation of Diffusion Policy: its reliance on a relatively large action horizon T_a , which compromises its responsiveness and adaptability to environmental changes.
- We propose Noise-Relaying Diffusion Policy (RNR-DP) which maintains a noise-relaying buffer with progressively increasing noise levels and employs a sequential denoising mechanism.
- We conduct extensive experiments on 5 tasks involving dynamic object manipulation and 4 simpler tasks that do not demand responsive control. The results consistently demonstrate that RNR-DP delivers both highly responsive and efficient control.

2 Related Work

Diffusion Model Acceleration Techniques Diffusion models (Ho et al., 2020) have garnered significant attention for their capacity to model complex distributions. However, their iterative sampling processes can

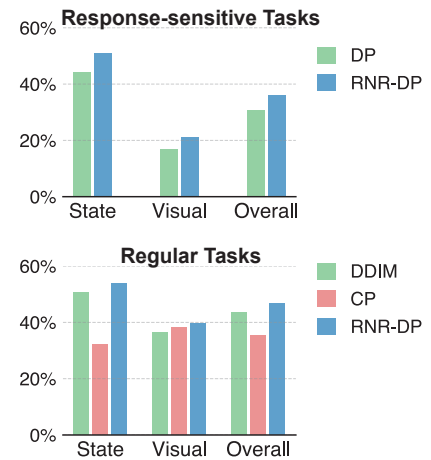


Figure 1: Our RNR-DP consistently delivers responsive and efficient control.

be computationally expensive due to the large number of diffusion steps required. One approach to address the low inference speed of diffusion models is by reducing the number of denoising steps needed, as seen in works like (Song et al., 2020) and (Karras et al., 2022). Another line of research employs distillation-based techniques, which begin with a pretrained teacher model and train a new student model to take larger steps over the ODE trajectories that the teacher has already learned to map, as demonstrated in (Song et al., 2023), (Liu et al., 2023), and (Salimans & Ho, 2022). Among the most commonly used acceleration techniques in the robotics community are DDIM (Song et al., 2020) and Consistency Models (Song et al., 2023), which are particularly effective for speeding up the diffusion policy process.

Diffusion Model for Motion Synthesis Diffusion Model, renowned for its strong representational capabilities, has been widely applied to motion synthesis tasks (Shafir et al., 2023). Building on this foundation, Zhang et al. (2024) proposed an innovative framework that incorporates temporally varying denoising and maintains a motion buffer comprising progressively noised poses, enabling long-term motion synthesis. Inspired by TEDi, we develop a noise-relaying buffer with incrementally increasing noise levels and implement a sequential denoising mechanism to enhance Diffusion Policy, ensuring more efficient and responsive control.

Diffusion Model as Policy With the success of diffusion models in image synthesis and video generation (Ho et al., 2020), they have become a popular choice as policy backbones in the robotics community. These models are utilized in two main ways: 1) As policies in reinforcement learning (RL) methods, including offline RL (Wang et al., 2022; Hansen-Estruch et al., 2023; Mao et al., 2024), offline-to-online RL (Ding & Jin, 2023), and online RL (Yang et al., 2023a); 2) As policies in imitation learning (Chi et al., 2023; Reuss et al., 2023). Diffusion Policy belongs to the second category and has demonstrated state-of-the-art performance compared to other imitation learning methods (Shafiullah et al., 2022; Florence et al., 2022; Abramson, 1970). Furthermore, it exhibits significant potential for future research and practical applications (Yuan et al., 2024).

3 Background

Diffusion Policy (Chi et al., 2023) models control policies using Denoising Diffusion Probabilistic Models (DDPMs) (Ho et al., 2020), which have shown strong performance in generative modeling. In control, Diffusion Policy predicts the future action sequence \mathbf{A}_t using a noise prediction network $\varepsilon_\theta(\mathbf{A}_t^{(k)}; \mathbf{O}_t, k)$, where $\mathbf{A}_t^{(k)} = \mathbf{A}_t + \epsilon^k$ is a perturbed version of the clean action sequence \mathbf{A}_t with added Gaussian noise ϵ at noise level k . The model learns to estimate and remove noise by minimizing the mean squared error (MSE) loss:

$$\mathcal{L} = \|\varepsilon_\theta(\mathbf{A}_t^{(k)}; \mathbf{O}, k) - \varepsilon^k\|^2.$$

During inference, given an observation \mathbf{O}_t , the trained network iteratively refines the action sequence over K denoising steps following:

$$\mathbf{A}_t^{(k-1)} = \alpha \left(\mathbf{A}_t^{(k)} - \gamma \varepsilon_\theta(\mathbf{A}_t^{(k)}; \mathbf{O}_t, k) + \epsilon \right),$$

where the initial action sequence \mathbf{A}_t is sampled from $\mathcal{N}(0, 1)$, and $\epsilon \sim \mathcal{N}(0, \sigma^2 I)$ represents Gaussian noise. The predefined noise schedule functions α, β , and σ are part of the DDPM scheduler (Ho et al., 2020). Once denoised to $\mathbf{A}_t^{(0)}$, the agent executes the first $n = T_a$ future steps after time t .

4 Limitations of Diffusion Policy

This section explores the key limitations of Diffusion Policy in detail. In summary, Diffusion Policy relies on a relatively large action horizon, T_a , to ensure a sequence of actions adheres to the same mode and avoid frequent mode bouncing. However, using a large action horizon results in most actions being unconditioned on the latest observations, thereby limiting the policy’s responsiveness to environmental changes. Section

Table 1: We compare the performance of Diffusion Policy under different action horizon T_a with multi-modal data and RL data.

Demo Type	Traj Num	Ta=1	Ta=2	Ta=4	Ta=8
Multi-Modal	1000	0.78	0.93	0.95	0.96
RL (Single-Modal)	500	0.62	0.59	0.58	0.55

4.1 delves into why Diffusion Policy requires a large action horizon, while Section 4.2 examines how this impacts responsiveness.

4.1 Why Diffusion Policy Needs A Large Action Horizon?

As shown in Chi et al. (2023), Diffusion Policy performs best with a relatively large action horizon T_a (e.g., $T_a = 8$), while $T_a = 1$ significantly degrades performance. This is because each action sequence is independently denoised from noise, and in multi-modal settings, $T_a = 1$ allows actions to switch modes, causing inconsistencies. Executing multiple actions within the same mode is crucial for stable performance. To validate this, we train Diffusion Policy on 500 single-modal demonstrations from an RL agent in the ManiSkill2 StackCube task. Results in Table 1 show no performance drop with $T_a = 1$, even slightly improving over $T_a = 8$, confirming that mode bouncing in multi-modal settings is the main reason for requiring a large action horizon.

4.2 How A Large Action Horizon Limits Responsiveness?

As discussed above, a large action horizon T_a is crucial for Diffusion Policy, particularly when modeling multi-modal data. However, an excessively large T_a can hinder responsiveness to rapid environmental changes. Consider a dexterous robotic hand tasked with picking up a ball from a surface and transporting it to a goal position. This task demands continuous fine-grained control and rapid adaptation to unforeseen disturbances, such as the ball slipping or shifting unpredictably within the fingers. If the policy commits to executing $T_a = 8$ future actions, it may struggle to react promptly to subtle variations in grip force or contact dynamics. For example, if the ball begins to slip, a long action sequence could delay corrective actions, making recovery difficult. In contrast, a short action horizon ($T_a = 1$) allows the policy to continuously refine its grip based on real-time feedback, ensuring stable and controlled relocation. This example highlights that in contact-rich object manipulation tasks, a large action horizon forces the policy to predict complex interactions prematurely, making precise control more challenging. Empirically, we observe that Diffusion Policy struggles with such dynamic, contact-rich manipulation tasks, where real-time adaptability is essential, further underscoring the dilemma between long-horizon consistency and responsiveness.

5 Responsive Noise-Relaying Diffusion Policy

To achieve responsive and efficient control, our proposed approach relies on a noise-relaying buffer and the implemented sequential denoising mechanism at its core (Section 5.1) with additional key design choices (Section 5.2). More details of the implementation including policy architecture and hyperparameters are summarized in Appendix B.

5.1 Noise-Relaying Buffer

The noise-relaying buffer $\tilde{\mathbf{Q}}_t = \{\mathbf{a}_t^{(1)}, \mathbf{a}_{t+1}^{(2)}, \dots, \mathbf{a}_{t+f-2}^{(f-1)}, \mathbf{a}_{t+f-1}^{(f)}\}$ contains a sequence of noisy actions with linearly increasing noise levels from 1 to f , where f is the buffer capacity as well as the total number of noise levels. As shown in Figure 2, after each denoising step, the trained network transforms $\tilde{\mathbf{Q}}_t$ into $\mathbf{Q}_t = \{\mathbf{a}_t^{(0)}, \mathbf{a}_{t+1}^{(1)}, \dots, \mathbf{a}_{t+f-2}^{(f-2)}, \mathbf{a}_{t+f-1}^{(f-1)}\}$, producing a noise-free action $\mathbf{a}_t^{(0)}$ at the head. This clean action is immediately executed, and a fully noisy action is appended to the buffer's tail. For the next step, the buffer

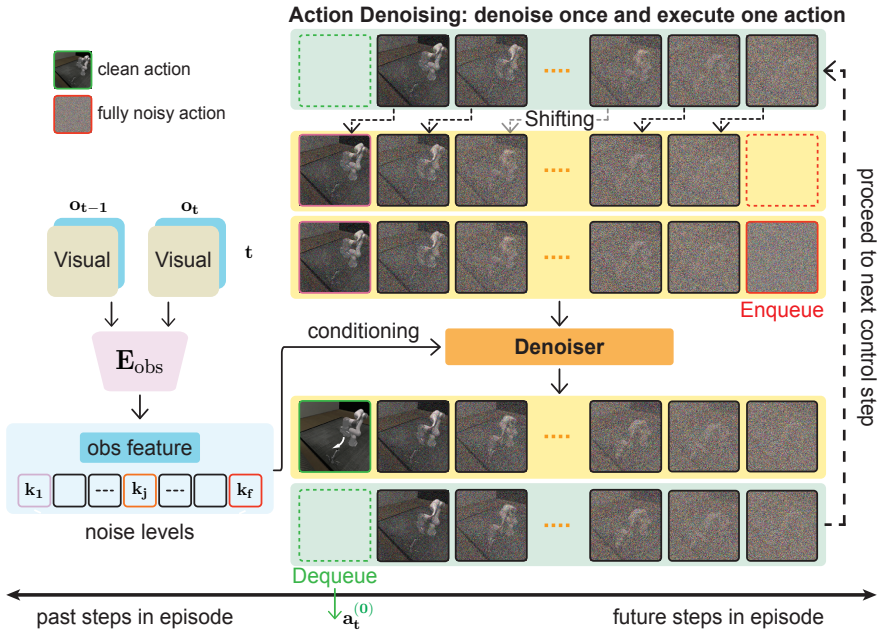


Figure 2: **Inference Overview of Responsive Noise-Relaying Diffusion Policy (RNR-DP).** The core of RNR-DP is the noise-relaying buffer (Section 5.1) and it has 3 stages during the entire control-loop, as exemplified by the transition between time step t and time step $t+1$, (1) The buffer contains noisy actions with increasing noise levels (2) After denoising once, each action in the buffer is denoised for one step, clean action at the buffer’s head is removed and executed (**dequeue**) (3) The remaining noisy actions are left shifted for one slot and a fully noisy action is appended to the buffer’s tail (**enqueue**). The conditioning data is discussed with more details in Section 5.2 and Appendix B.3.

reuses $f - 1$ denoising steps from previous outputs, ensuring consistency and avoiding full denoising from scratch. This sequential denoising mechanism conditions clean actions on the latest observations, enabling responsive and long-term active control. Pseudocode is provided in Algorithm 1.

5.2 Key Design Choices

Mixture Noise Scheduling We train the denoiser network following the DDPM (Ho et al., 2020) framework, and allow each action in \mathbf{A}_t perturbed by independent noise levels. Given a fixed variance schedule β_1, \dots, β_f ($\beta_1 < \beta_f$), any \mathbf{a}_j in \mathbf{A}_t can be perturbed by one of the f levels. During training, we use a mixed per-action noise injection scheme (*mixture schedule*): with probability p_{linear} , actions are perturbed by linearly increasing variances (*linear schedule*); with probability $1 - p_{\text{linear}}$, actions are perturbed by random variances from β_1 to β_f (*random schedule*). The *random schedule* trains the model to denoise actions independently $p_\theta(\mathbf{a}^{(k-1)} | \mathbf{a}^{(k)}; \mathbf{O}), 1 \leq k \leq f$, while the *linear schedule* ensures smooth transitions across consecutive actions during inference. Unlike Diffusion Policy, which applies a single variance level to all actions in \mathbf{A}_t per iteration, our mixture schedule enables diverse and robust training.

Laddering Initialization During inference, we use a noise-relaying buffer with f noisy action frames, following Algorithm 1. Initially, the buffer contains f fully noisy actions sampled from $\mathcal{N}(\mathbf{0}, \mathbf{I})$, i.e., $\tilde{\mathbf{Q}} = \{\mathbf{z}_j \sim \mathcal{N}(\mathbf{0}, \mathbf{I}) \mid j = 1, \dots, f\}$. To align with training and avoid performance drops, we initialize the buffer by iteratively denoising it f times using the *random schedule* conditioned on the initial observation \mathbf{O}_0 . This transforms the buffer to follow the *linear schedule*, ensuring smooth and responsive control. Since this process transitions the buffer from uniform noise to monotonically increasing variances like a ladder, we term it *laddering initialization*, as illustrated in Figure 3.

Noise-Aware Conditioning Unlike Diffusion Policy (Chi et al., 2023), which encodes a single diffusion step to one time embedding, our approach uses mixed scheduling and a noise-relaying buffer to handle multiple

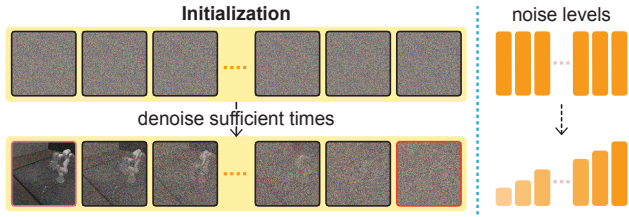


Figure 3: **A visualization of the initialization process.** Noise-relaying buffer contains only fully noisy actions sampled from standard multivariate Gaussian distribution of dimension T_a at each action index before the initialization; the buffer is denoised for f times until the buffer head contains minimal noise level and can be executed with one more model forward call.

noise levels, requiring awareness of multiple diffusion steps. For each action’s noise level k_j ($1 \leq k_j \leq f$), we use an MLP to encode a time embedding, yielding f embeddings. These are appended to the observation features from the encoder E_{obs} . This allows the buffer, during both training and inference, to decode actions at each noise level using up-to-date observations, enabling more dynamic and consistent behaviors. See Appendix B.3 for more details.

6 Experiments

The goal of our experimental evaluation is to study the following questions:

1. Can Responsive Noise-Relaying Diffusion Policy outperform Diffusion Policy by delivering more responsive control? (Section 6.3)?
2. Can Responsive Noise-Relaying Diffusion Policy function as a superior acceleration method compared to commonly used alternatives on simpler tasks that do not require responsive control (Section 6.4)?
3. What are the effects of the components introduced by Responsive Noise-Relaying Diffusion Policy (Section 6.5)?

6.1 Experimental Setup



Figure 4: **Task Visualization in Simulation.** ManiSkill tasks including PushT, RollBall, PushChair, StackCube, TurnFaucet; Adroit tasks including Relocate, Door, Pen, Hammer. See Appendix A.1 for more properties about each task.

To validate the responsiveness and efficiency of Responsive Noise-Relaying Diffusion Policy, our experimental setup incorporates *variations in the following dimensions*:

- **Task Types:** Stationary robot arm manipulation, mobile manipulation, dual-arm coordination, dexterous hand manipulation, articulated object manipulation, and high-precision tasks.
- **Demo Sources:** Teleoperation, Task and Motion Planning, RL, and Model Predictive Control.
- **Observation Modalities:** State observation (low-dim) and visual observation (high-dim).

6.1.1 Task Descriptions

Our experiments are conducted on 9 tasks from 3 benchmarks: ManiSkill2 (robotic manipulation; 3 tasks), ManiSkill3 (robotic manipulation; 2 tasks) and Adroit (dexterous manipulation; 4 tasks). These tasks are separated into 2 groups to validate the responsiveness and efficiency of Responsive Noise-Relaying Diffusion Policy.

Response-sensitive Group: Tasks Involving Dynamic Object Manipulation Requiring Responsive Control We consider 5 challenging tasks involving contact-rich, dynamic object manipulation to assess the responsiveness of RNR-DP. PushT requires using a stick to push a T-shaped block to a target location and orientation. RollBall involves pushing and rolling a ball to a randomized goal region. PushChair tests bimanual manipulation of articulated objects with variations. Adroit Relocate involves picking up a ball and moving it to a goal position, while Adroit Door requires unlocking and opening a door. See Figure 4 for task visualizations, and more details are included in Appendix A.1.

Regular Group: Simpler Tasks that Do Not Require Responsive Control We consider the rest 4 simpler tasks that do not require responsive control to validate the efficiency of RNR-DP. StackCube requires picking up a cube and stack it onto another cube. TurnFaucet uses a stationary arm to turn on faucets of various geometries and topology. Adroit Pen repositions the blue pen to match the orientation of the green target. Adroit Hammer picks up a hammer and drives a nail into a board. More details are included in Appendix A.1.

6.2 Baselines

We compare our Responsive Noise-Relaying Diffusion Policy against a set of strong baselines related to Diffusion Policy.

Diffusion Policy (DDPM) is the original setting from [Chi et al. \(2023\)](#), which utilizes a conditional Denoising Diffusion Probabilistic Model with discrete time scheduling to generate actions. We use 100 DDPM denoising steps in our experiments.

Diffusion Policy (EDM) is introduced in [Prasad et al. \(2024\)](#) to train a teacher model and employs the EDM ([Karras et al., 2022](#)) framework with continuous-time scheduling. This model takes the current position x_t , time t , and conditioning o as inputs along a PFODE and is used to estimate the derivative of the PFODE's trajectory. We utilize the EDM model with Heun's second-order solver taking 80 denoising steps, which requires two neural network evaluations per discretized step in the ODE, resulting in a total of 159 neural function evaluations (**NFEs**).

Diffusion Policy (DDIM) is used in [Chi et al. \(2023\)](#) to accelerate Diffusion Policy with Diffusion Denoising Implicit Model framework ([Song et al., 2020](#)). We test 1, 2, 4, and 8 DDIM denoising steps.

Consistency Policy (CP) is introduced in [Prasad et al. \(2024\)](#), which employs the Consistency Trajectory Model ([Kim et al., 2023](#)) to distill the knowledge from a Teacher Model (EDM). We evaluate both the 1-step Consistency Policy and the 8-step chaining Consistency Policy.

Streaming Diffusion Policy (SDP) is a recent advancement over Diffusion Policy that stays close to our approach. See Appendix C.2 for detailed discussion.

6.3 Results & Analysis on Responsive Control

First, we provide comprehensive evaluation and validate the responsiveness of RNR-DP on 5 tasks (Response-sensitive Group) involving contact-rich dynamic object manipulation, a primary focus of our policy. Figure 1 shows an overview of performance improvement. As shown in Table 2 and Table 3, RNR-DP consistently outperforms Diffusion Policy across all tested scenarios in both state and visual experiments. Specifically, in state experiments, RNR-DP achieves a 15.1% improvement over Diffusion Policy, while in visual experiments, it demonstrates a 24.9% improvement. Overall, RNR-DP surpasses Diffusion Policy by 18.0%. Notably, in the Relocate task, RNR-DP achieves a significant performance boost of 38.6% over Diffusion Policy.

Table 2: Evaluation on tasks requiring responsive control (Response-sensitive Group) from ManiSkill and Adroit benchmarks (State Observations). We report average success rate (\uparrow) of the best checkpoint for 1000 episodes across 10 random seeds. Results that are statistically better are highlighted in **bold**. Our results are highlighted in **light-blue** cells.

Method	Relocate	Door	PushChair	RollBall	PushT
	w/ g	w/o g			
DP	0.422	0.558	0.495	0.635	0.083
RNR-DP	0.585	0.629	0.547	0.694	0.121
					0.491

Table 3: Evaluation on tasks (Response-sensitive Group) from ManiSkill and Adroit benchmarks (Visual Observations). We report values under the same settings as in Table 2. Tasks in which none of the methods achieve a reasonable success rate under visual observations are omitted.

Method	Door (Adroit)	RollBall (MS3)	PushT (MS3)
DP	0.079	0.080	0.349
RNR-DP	0.122	0.131	0.379

We attribute these significant performance gains to the design of our noise-relaying buffer and sequential denoising mechanism, which offer two key advantages. The noise-relaying buffer ensures that the denoising of each action remains consistent, allowing actions to follow the same mode. This effectively eliminates frequent mode bouncing, enabling RNR-DP to support single-action rollouts ($T_a = 1$). Furthermore, the single-action rollout in RNR-DP ensures that all actions are conditioned on the latest observations, resulting in significantly more responsive control to environmental changes compared to Diffusion Policy.

6.4 Results & Analysis on Efficient Control

In this section, we conduct extended experiments on 4 simpler tasks (Regular Group) that do not require responsive control to evaluate the efficiency of RNR-DP. An overview of the performance improvements is provided in Figure 1. Section 6.4.1 introduces a metric designed for fair efficiency comparisons, while Section 6.4.2 provides a detailed analysis of the empirical results compared to commonly used acceleration methods.

6.4.1 Neural Function Evaluations per Action (NFEs/a)

Adopting the settings from Chi et al. (2023), Diffusion Policy and related methods utilize a relatively large action horizon (T_a) to achieve better performance, whereas RNR-DP employs a single-action rollout ($T_a = 1$) at each inference. To facilitate a fair comparison of efficiency, we introduce a new metric, **Neural Function Evaluations per Action (NFEs/a)**, as defined in Equation (1).

$$\text{NFEs/a} = \frac{\text{NFEs}}{T_a} \quad (1)$$

6.4.2 Empirical Comparison with Commonly Used Acceleration Methods

To evaluate the efficiency of Responsive Noise-Relaying Diffusion Policy (RNR-DP), we compare it against common acceleration methods, including DDIM (Chi et al., 2023) and Consistency Policy (Prasad et al., 2024), on simpler tasks that do not require responsive control (Regular Group). As shown in Table 4 and Appendix C.1, RNR-DP consistently achieves the highest overall performance among all DDIM and Consistency Policy variants. For a fair comparison, we specifically evaluate RNR-DP against 8-step DDIM (NFEs/a = 1) and 8-step-chaining Consistency Policy (NFEs/a = 1). In state-based experiments, RNR-DP outperforms 8-step DDIM by 5.7% and 8-step-chaining Consistency Policy by 66.2%. In vision-based experi-

Table 4: Evaluation on simpler tasks (Regular Group) not requiring responsive control from ManiSkill and Adroit benchmarks (State Observations). We report average success rate (\uparrow) and overall average success rate of all tasks (\uparrow). Particularly, DDIMs with NFEs/a = 1, CPs with NFEs/a = 1 are highlighted in **light-green**, **light-red** cells respectively. Our results are highlighted in **light-blue** cells.

Method	Steps (S)	NFEs/a	StackCube		TurnFaucet		Pen	Hammer	Avg. SR of tasks
			w/ g	w/o g	0.495	0.595			
DDPM	100	12.5	0.960	0.495	0.595	0.508	0.120	0.000	0.536
	1	0.125	0.000	0.000	0.000	0.110	0.000	0.000	0.000
DDIM	2	0.25	0.214	0.433	0.594	0.190	0.000	0.000	0.286
	4	0.5	0.959	0.482	0.612	0.476	0.000	0.000	0.506
EDM	8	1	0.964	0.477	0.614	0.483	0.000	0.000	0.508
	80	20	0.955	0.449	0.575	0.517	0.120	0.000	0.523
CP	1	0.125	0.214	0.051	0.028	0.326	0.000	0.000	0.124
	8	1	0.680	0.112	0.299	0.483	0.041	0.041	0.323
RNR-DP	1	1	0.935	0.531	0.594	0.487	0.139	0.139	0.537

Table 5: Ablation study on noise scheduling scheme during training (Section 5.2). Numbers represent average success rates (\uparrow). Numbers in parenthesis indicate the performance drop after removing key component of our Responsive Noise-Relaying Diffusion Policy.

Ablation	Relocate (Adroit)	Door (Adroit)
	0.323 (-26.2%)	0.404 (-22.5%)
Linear	0.389 (-19.6%)	0.360 (-26.9%)
Random	0.585	0.629
Mixture (Ours)		

ments, it surpasses 8-step DDIM by 8.5% and 8-step-chaining Consistency Policy by 3.4%, yielding an overall improvement of 6.9% over 8-step DDIM and 32.0% over 8-step-chaining Consistency Policy. Additionally, both DDIM and Consistency Policy struggle in certain tasks. For instance, 8-step DDIM achieves a 0% success rate on Adroit Hammer, while Consistency Policy performs poorly on StackCube and TurnFaucet. In contrast, RNR-DP demonstrates consistent and robust performance across all tasks. Notably, RNR-DP achieves an average success rate comparable to Diffusion Policy across all state and visual experiments while being 12.5 times faster. These results confirm that even on simpler tasks, RNR-DP serves as a superior acceleration method, enabling efficient control.

We attribute this robust performance to the design of the noise-relaying buffer and sequential denoising mechanism. By reusing denoising steps from previous outputs, RNR-DP requires only one denoising step to generate a single action, while ensuring all actions undergo sufficient denoising to maintain high action quality. In contrast, DDIM and Consistency Policy significantly reduce the number of denoising steps per action, leading to pronounced performance drops.

6.5 Ablation Study

We conduct various ablations to provide further insights on the effects of components of RNR-DP.

Noise Scheduling Scheme We conduct a comprehensive study to evaluate how different noise scheduling schemes impact the performance of the Responsive Noise-Relaying Diffusion Policy. As shown in Table 5, the results demonstrate that relying solely on either a *linear schedule* or a *random schedule* significantly reduces task success rates. This highlights the importance of integrating *mixture scheduling* to fully exploit the potential of the noise-relaying buffer design. By combining the two schedules, our model effectively utilizes different noise levels, enhancing the robustness and adaptability of action generation.

Table 6: Ablation study on noise-relaying buffer initialization (Section 5.2).

Ablation	Relocate (Adroit)	Door (Adroit)
Pure noise	0.522 (-6.3%)	0.516 (-11.3%)
Laddering (Ours)	0.585	0.629

Table 7: Ablation study on model prediction type (Section 5.2).

Ablation	Relocate (Adroit)	Door (Adroit)
Action	0.154 (-43.1%)	0.374 (-25.5%)
Noise (Ours)	0.585	0.629

Noise-Relaying Buffer Initialization We conduct an ablation study to evaluate the effectiveness of our initialization scheme. *Pure noise* directly uses a fully noisy buffer as the initialization for subsequent operations. As shown in Table 6, *laddering initialization* achieves significant performance gains compared to *pure noise*. This result highlights the critical role of our initialization scheme in enabling strong and robust performance.

Noise-Relaying Buffer Capacity We also evaluate the impact of the noise-relaying buffer capacity to the performance, the only tuned hyperparameter in our approach. As shown in Figure 5, on the Adroit Relocate task, RNR-DP achieves peak performance of 58.5% at a buffer capacity of 84 and maintains strong performance within the range of 56 to 92, demonstrating a wide tolerance. Performance declines when the buffer capacity is too small (e.g., 48) or too large (e.g., 100). Notably, Diffusion Policy achieves only 42.2%, while RNR-DP with buffer capacities between 48 and 100 consistently outperforms it.

This highlights that for a single task, the noise-relaying buffer offers robust performance over a broad range and is not difficult to tune. Empirically, starting with a value between 56 and 84 and making adjustments suffices most cases.

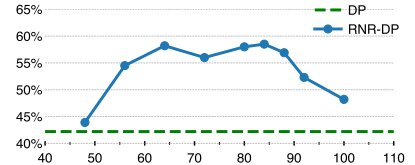


Figure 5: Noise-relaying buffer capacity v.s. average success rate.

Model Prediction Type In addition, we investigate the impact of the model’s prediction type. As shown in Table 7, models predicting the added noise component outperform those directly predicting the action sequence. This finding aligns with the common practice of using noise prediction in diffusion models within the vision domain (Ho et al., 2020).

7 Conclusion and Future Work

In this paper, we identify the key limitation of Diffusion Policy: its reliance on a relatively large action horizon T_a compromises its responsiveness and adaptability to environment changes. To address these issues, we propose Responsive Noise-Relaying Diffusion Policy which maintains a noise-relaying buffer with progressively increasing noise levels and employs a sequential denoising mechanism. Our method provides more responsive control than Diffusion Policy on 5 tasks involving dynamic object manipulation, and delivers more efficient control than commonly used acceleration methods on 4 simpler tasks.

Limitations. A limitation of this work is the lack of additional experiments to demonstrate whether our method preserves behavioral diversity compared to Diffusion Policy. This remains an area for future research.

References

- Norman Abramson. The aloha system: Another alternative for computer communications. In *Proceedings of the November 17-19, 1970, fall joint computer conference*, pp. 281–285, 1970.
- Firas Al-Hafez, Guoping Zhao, Jan Peters, and Davide Tateo. Locomujoco: A comprehensive imitation learning benchmark for locomotion. *arXiv preprint arXiv:2311.02496*, 2023.
- Lili Chen, Kevin Lu, Aravind Rajeswaran, Kimin Lee, Aditya Grover, Misha Laskin, Pieter Abbeel, Aravind Srinivas, and Igor Mordatch. Decision transformer: Reinforcement learning via sequence modeling. *Advances in neural information processing systems*, 34:15084–15097, 2021.
- Cheng Chi, Zhenjia Xu, Siyuan Feng, Eric Cousineau, Yilun Du, Benjamin Burchfiel, Russ Tedrake, and Shuran Song. Diffusion policy: Visuomotor policy learning via action diffusion. *The International Journal of Robotics Research*, pp. 02783649241273668, 2023.
- Zihan Ding and Chi Jin. Consistency models as a rich and efficient policy class for reinforcement learning. *arXiv preprint arXiv:2309.16984*, 2023.
- Yuqing Du, Daniel Ho, Alex Alemi, Eric Jang, and Mohi Khansari. Bayesian imitation learning for end-to-end mobile manipulation. In *International Conference on Machine Learning*, pp. 5531–5546. PMLR, 2022.
- Pete Florence, Corey Lynch, Andy Zeng, Oscar A Ramirez, Ayzaan Wahid, Laura Downs, Adrian Wong, Johnny Lee, Igor Mordatch, and Jonathan Tompson. Implicit behavioral cloning. In *Conference on Robot Learning*, pp. 158–168. PMLR, 2022.
- Jiayuan Gu, Fanbo Xiang, Xuanlin Li, Zhan Ling, Xiqiang Liu, Tongzhou Mu, Yihe Tang, Stone Tao, Xinyue Wei, Yunchao Yao, Xiaodi Yuan, Pengwei Xie, Zhiao Huang, Rui Chen, and Hao Su. Maniskill2: A unified benchmark for generalizable manipulation skills. In *The Eleventh International Conference on Learning Representations, ICLR 2023, Kigali, Rwanda, May 1-5, 2023*. OpenReview.net, 2023. URL https://openreview.net/forum?id=b_CQDy9vrD1.
- Philippe Hansen-Estruch, Ilya Kostrikov, Michael Janner, Jakub Grudzien Kuba, and Sergey Levine. Idql: Implicit q-learning as an actor-critic method with diffusion policies. *arXiv preprint arXiv:2304.10573*, 2023.
- Jonathan Ho, Ajay Jain, and Pieter Abbeel. Denoising diffusion probabilistic models. *Advances in neural information processing systems*, 33:6840–6851, 2020.
- Sigmund H. Høeg, Yilun Du, and Olav Egeland. Streaming diffusion policy: Fast policy synthesis with variable noise diffusion models, 2024. URL <https://arxiv.org/abs/2406.04806>.
- Edward Johns. Coarse-to-fine imitation learning: Robot manipulation from a single demonstration. In *2021 IEEE international conference on robotics and automation (ICRA)*, pp. 4613–4619. IEEE, 2021.
- Tero Karras, Miika Aittala, Timo Aila, and Samuli Laine. Elucidating the design space of diffusion-based generative models. *Advances in neural information processing systems*, 35:26565–26577, 2022.
- Dongjun Kim, Chieh-Hsin Lai, Wei-Hsiang Liao, Naoki Murata, Yuhta Takida, Toshimitsu Uesaka, Yutong He, Yuki Mitsufuji, and Stefano Ermon. Consistency trajectory models: Learning probability flow ode trajectory of diffusion. *arXiv preprint arXiv:2310.02279*, 2023.
- Xingchao Liu, Xiwen Zhang, Jianzhu Ma, Jian Peng, et al. Instaflow: One step is enough for high-quality diffusion-based text-to-image generation. In *The Twelfth International Conference on Learning Representations*, 2023.
- Liyuan Mao, Haoran Xu, Xianyuan Zhan, Weinan Zhang, and Amy Zhang. Diffusion-dice: In-sample diffusion guidance for offline reinforcement learning. *arXiv preprint arXiv:2407.20109*, 2024.

-
- Ethan Perez, Florian Strub, Harm De Vries, Vincent Dumoulin, and Aaron Courville. Film: Visual reasoning with a general conditioning layer. In *Proceedings of the AAAI conference on artificial intelligence*, volume 32, 2018.
- Aaditya Prasad, Kevin Lin, Jimmy Wu, Linqi Zhou, and Jeannette Bohg. Consistency policy: Accelerated visuomotor policies via consistency distillation. *arXiv preprint arXiv:2405.07503*, 2024.
- Yuzhe Qin, Yueh-Hua Wu, Shaowei Liu, Hanwen Jiang, Ruihan Yang, Yang Fu, and Xiaolong Wang. Dexmv: Imitation learning for dexterous manipulation from human videos. In *European Conference on Computer Vision*, pp. 570–587. Springer, 2022.
- Ilija Radosavovic, Xiaolong Wang, Lerrel Pinto, and Jitendra Malik. State-only imitation learning for dexterous manipulation. In *2021 IEEE/RSJ International Conference on Intelligent Robots and Systems (IROS)*, pp. 7865–7871. IEEE, 2021.
- Aravind Rajeswaran, Vikash Kumar, Abhishek Gupta, Giulia Vezzani, John Schulman, Emanuel Todorov, and Sergey Levine. Learning complex dexterous manipulation with deep reinforcement learning and demonstrations. *arXiv preprint arXiv:1709.10087*, 2017.
- Nathan Ratliff, J Andrew Bagnell, and Siddhartha S Srinivasa. Imitation learning for locomotion and manipulation. In *2007 7th IEEE-RAS international conference on humanoid robots*, pp. 392–397. IEEE, 2007.
- Moritz Reuss, Maximilian Li, Xiaogang Jia, and Rudolf Lioutikov. Goal-conditioned imitation learning using score-based diffusion policies. *arXiv preprint arXiv:2304.02532*, 2023.
- Tim Salimans and Jonathan Ho. Progressive distillation for fast sampling of diffusion models. *arXiv preprint arXiv:2202.00512*, 2022.
- Yonatan Shafir, Guy Tevet, Roy Kapon, and Amit H Bermano. Human motion diffusion as a generative prior. *arXiv preprint arXiv:2303.01418*, 2023.
- Nur Muhammad Shafullah, Zichen Cui, Ariuntuya Arty Altanzaya, and Lerrel Pinto. Behavior transformers: Cloning k modes with one stone. *Advances in neural information processing systems*, 35:22955–22968, 2022.
- Jiaming Song, Chenlin Meng, and Stefano Ermon. Denoising diffusion implicit models. *arXiv preprint arXiv:2010.02502*, 2020.
- Yang Song, Prafulla Dhariwal, Mark Chen, and Ilya Sutskever. Consistency models. *arXiv preprint arXiv:2303.01469*, 2023.
- Simon Stepputtis, Joseph Campbell, Mariano Phielipp, Stefan Lee, Chitta Baral, and Heni Ben Amor. Language-conditioned imitation learning for robot manipulation tasks. *Advances in Neural Information Processing Systems*, 33:13139–13150, 2020.
- Stone Tao, Fanbo Xiang, Arth Shukla, Yuzhe Qin, Xander Hinrichsen, Xiaodi Yuan, Chen Bao, Xinsong Lin, Yulin Liu, Tse kai Chan, Yuan Gao, Xuanlin Li, Tongzhou Mu, Nan Xiao, Arnav Gurha, Zhiao Huang, Roberto Calandra, Rui Chen, Shan Luo, and Hao Su. Maniskill3: Gpu parallelized robotics simulation and rendering for generalizable embodied ai, 2024. URL <https://arxiv.org/abs/2410.00425>.
- Zhendong Wang, Jonathan J Hunt, and Mingyuan Zhou. Diffusion policies as an expressive policy class for offline reinforcement learning. *arXiv preprint arXiv:2208.06193*, 2022.
- Josiah Wong, Albert Tung, Andrey Kurenkov, Ajay Mandlekar, Li Fei-Fei, Silvio Savarese, and Roberto Martín-Martín. Error-aware imitation learning from teleoperation data for mobile manipulation. In *Conference on Robot Learning*, pp. 1367–1378. PMLR, 2022.
- Fan Xie, Alexander Chowdhury, M De Paolis Kaluza, Linfeng Zhao, Lawson Wong, and Rose Yu. Deep imitation learning for bimanual robotic manipulation. *Advances in neural information processing systems*, 33:2327–2337, 2020.

Long Yang, Zhixiong Huang, Fenghao Lei, Yucun Zhong, Yiming Yang, Cong Fang, Shiting Wen, Binbin Zhou, and Zhouchen Lin. Policy representation via diffusion probability model for reinforcement learning. *arXiv preprint arXiv:2305.13122*, 2023a.

Ruihan Yang, Zhuoqun Chen, Jianhan Ma, Chongyi Zheng, Yiyu Chen, Quan Nguyen, and Xiaolong Wang. Generalized animal imitator: Agile locomotion with versatile motion prior. *arXiv preprint arXiv:2310.01408*, 2023b.

Xiu Yuan, Tongzhou Mu, Stone Tao, Yunhao Fang, Mengke Zhang, and Hao Su. Policy decorator: Model-agnostic online refinement for large policy model. *arXiv preprint arXiv:2412.13630*, 2024.

Zihan Zhang, Richard Liu, Kfir Aberman, and Rana Hanocka. Tedi: Temporally-entangled diffusion for long-term motion synthesis. In *SIGGRAPH, Technical Papers*, 2024. doi: 10.1145/3641519.3657515.

A Further Details on the Experimental Setup

A.1 Task Descriptions

We consider a total of 9 continuous control tasks from 3 benchmarks: ManiSkill2 (Gu et al., 2023), ManiSkill3 (Tao et al., 2024), and Adroit (Rajeswaran et al., 2017). This section provides detailed task descriptions on overall information, task difficulty, object sets, state space, and action space. Some task details are listed in Table 8.

Table 8: We consider 9 continuous tasks from 3 benchmarks. We list important task details below.

Task	State Obs Dim	C_{state}	Act Dim	C_a	Max Episode	Step
ManiSkill3: PushT	31		7		100	
ManiSkill3: RollBall	44		4		80	
ManiSkill2: StackCube	55		4		200	
ManiSkill2: TurnFaucet	43		7		200	
ManiSkill2: PushChair	131		20		200	
Adroit: Door	39		28		300	
Adroit: Pen	46		24		200	
Adroit: Hammer	46		26		400	
Adroit: Relocate	39		30		400	

A.1.1 ManiSkill2 Tasks

StackCube

- Overall Description: Pick up a red cube and place it onto a green one. See Figure 6 for episode visualization.
- Task Difficulty: This task requires precise control. The gripper needs to firmly grasp the red cube and accurately place it onto the green one.
- Object Variations: No object variations
- Action Space: Delta position of the end-effector and joint positions of the gripper.
- State Observation Space: Proprioceptive robot state information, such as joint angles and velocities of the robot arm, and task-specific goal information
- Visual Observation Space: one 64x64 RGBD image from a base camera and one 64x64 RGBD image from a hand camera.



Figure 6: StackCube Episode Visualization.

TurnFaucet

- Overall Description: Turn on a faucet by rotating its handle.
- Task Difficulty: This task needs to handle object variations. See Figure 7 for episode visualization.

- Object Variations: We have a source environment containing 10 faucets, and the dataset is collected in the source environment. w/o g means the agent directly interacts with the source environment online; w/ g means the agent interacts with the target environment online, which contains 4 novel faucets.
- Action Space: Delta pose of the end-effector and joint positions of the gripper.
- State Observation Space: Proprioceptive robot state information, such as joint angles and velocities of the robot arm, the mobile base, and task-specific goal information.



Figure 7: TurnFaucet Episode Visualization.

PushChair

- Overall Description: A dual-arm mobile robot needs to push a swivel chair to a target location on the ground (indicated by a red hemisphere) and prevent it from falling over. The friction and damping parameters for the chair joints are randomized. See Figure 8 for episode visualization.
- Task Difficulty: This task needs to handle object variations.
- Object Variations: We have a source environment containing 5 chairs, and the dataset is collected in the source environment. w/o g means the agent directly interacts with the source environment online; w/ g means the agent interacts with the target environment online, which contains 3 novel faucets.
- State Observation Space: Proprioceptive robot state information, such as joint angles and velocities of the robot arm, task-specific goal information.
- Visual Observation Space: three 50x125 RGBD images from three cameras 120° apart from each other mounted on the robot.



Figure 8: PushChair Episode Visualization.

A.1.2 ManiSkill3 Tasks

PushT

- Overall Description: It is a simulated version of the real-world push-T task from Diffusion Policy: <https://diffusion-policy.cs.columbia.edu/>. In this task, the robot needs to precisely push the T-shaped block into the target region, and move the end-effector to the end-zone which terminates the episodes. The success condition is that the T block covers 90% of the 2D goal T's area. See Figure 9 for episode visualization.
- Task Difficulty: The task involves manipulating a dynamic T-shaped object, which introduces non-linear dynamics, friction, and contact forces.
- Object Variations: No object variations.

- Action Space: Delta pose of the end-effector and joint positions of the gripper.
- State Observation Space: Proprioceptive robot state information, such as joint angles and velocities of the robot arm, and task-specific goal information.
- Visual Observation Space: one 64x64 RGBD image from a base camera.

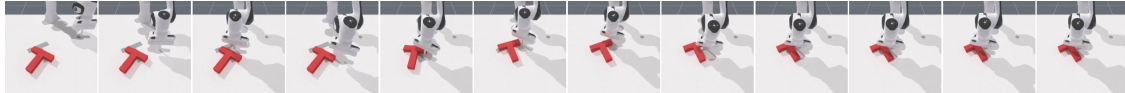


Figure 9: PushT Episode Visualization. The T-Block is pushed from sampled initial configuration to the goal area.

RollBall

- Overall Description: A task where the objective is to push and roll a ball to a goal region at the other end of the table. The success condition is that The ball's xy position is within goal radius (default 0.1) of the target's xy position by euclidean distance. See Figure 10 for episode visualization.
- Task Difficulty: The task involves manipulating a dynamic ball, which introduces non-linear dynamics, friction, and contact forces.
- Object Variations: No object variations.
- Action Space: Delta position of the end-effector and joint positions of the gripper.
- State Observation Space: Proprioceptive robot state information, such as joint angles and velocities of the robot arm, and task-specific goal information.
- Visual Observation Space: one 64x64 RGBD image from a base camera.



Figure 10: Rollball Episode Visualization. The blue ball is pushed and rolled from sampled initial configuration to the target red circle.

A.1.3 Adroit Tasks

Adroit Door

- Overall Description: The environment is based on the Adroit manipulation platform, a 28 degree of freedom system which consists of a 24 degrees of freedom ShadowHand and a 4 degree of freedom arm. The task to be completed consists on undoing the latch and swing the door open. See Figure 11 for episode visualization.
- Task Difficulty: The latch has significant dry friction and a biass torque that forces the door to stay closed. No information about the latch is explicitly provided. The position of the door is randomized.
- Object Variations: No object variations.
- Action Space: Absolute angular positions of the Adroit hand joints.



Figure 11: Door Episode Visualization.

- State Observation Space: The angular position of the finger joints, the pose of the palm of the hand, as well as state of the latch and door.
- Visual Observation Space: one 128x128 RGB image from a third-person view camera.

Adroit Pen

- Overall Description: The environment is based on the Adroit manipulation platform, a 28 degree of freedom system which consists of a 24 degrees of freedom ShadowHand and a 4 degree of freedom arm. The task to be completed consists on repositioning the blue pen to match the orientation of the green target. See Figure 12 for episode visualization.
- Task Difficulty: The target is also randomized to cover all configurations.
- Object Variations: No object variations.
- Action Space: Absolute angular positions of the Adroit hand joints.
- State Observation Space: The angular position of the finger joints, the pose of the palm of the hand, as well as the pose of the real pen and target goal.
- Visual Observation Space: one 128x128 RGB image from a third-person view camera.

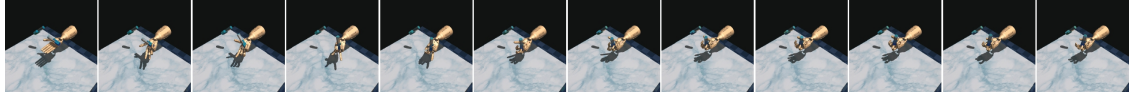


Figure 12: Pen Episode Visualization.

Adroit Hammer

- Overall Description: The environment is based on the Adroit manipulation platform, a 28 degree of freedom ShadowHand and a 4 degree of freedom arm. The task to be completed consists on picking up a hammer with and drive a nail into a board. See Figure 13 for episode visualization.
- Task Difficulty: The nail position is randomized and has dry friction capable of absorbing up to 15N force.
- Object Variations: No object variation.
- Action Space: Absolute angular positions of the Adroit hand joints.
- State Observation Space: The angular position of the finger joints, the pose of the palm of the hand, the pose of the hammer and nail, and external forces on the nail.
- Visual Observation Space: one 128x128 RGB image from a third-person view camera.

Adroit Relocate

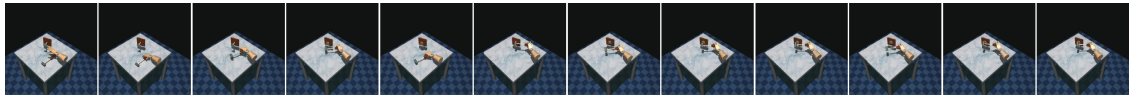


Figure 13: Hammer Episode Visualization.

- Overall Description: The environment is based on the Adroit manipulation platform, a 30 degree of freedom system which consists of a 24 degrees of freedom ShadowHand and a 6 degree of freedom arm. The task to be completed consists on moving the blue ball to the green target. See Figure 14 for episode visualization.
- Task Difficulty: The positions of the ball and target are randomized over the entire workspace.
- Object Variations: No object variations.
- Action Space: Absolute angular positions of the Adroit hand joints.
- State Observation Space: The angular position of the finger joints, the pose of the palm of the hand, as well as kinematic information about the ball and target.
- Visual Observation Space: one 128x128 RGB image from a third-person view camera.



Figure 14: Relocate Episode Visualization.

A.2 Demonstrations

This subsection provides the details of demonstrations used in our experiments. See Table 9. ManiSkill2 and ManiSkill3 demonstrations are provided in [Gu et al. \(2023\)](#) and [Tao et al. \(2024\)](#), and Adroit demonstrations are provided in [Rajeswaran et al. \(2017\)](#).

Table 9: Demonstration sources, numbers and generation methods.

Task	Traj Num for Training	Generation Method
ManiSkill3: PushT	1000	Reinforcement Learning
ManiSkill3: RollBall	1000	Reinforcement Learning
ManiSkill2: StackCube	1000	Task & Motion Planning
ManiSkill2: TurnFaucet	1000	Model Predictive Control
ManiSkill2: PushChair	1000	Reinforcement Learning
Adroit: Door	25	Human Demonstration
Adroit: Pen	25	Human Demonstration
Adroit: Hammer	25	Human Demonstration
Adroit: Relocate	25	Human Demonstration

B Implementation Details

B.1 Noise-Relying Diffusion Policy Inference

We summarize the inference pseudo-code of our RNR-DP in Algorithm 1.

Algorithm 1 Noise-relaying Diffusion Policy Inference

```

1: Require: denoising model,  $\varepsilon_\theta$ ; observation,  $\mathbf{O}_t$ ; noise-relaying buffer,  $\tilde{\mathbf{Q}}_t$ ; buffer capacity  $f$ ;
2: while task execution do
3:    $\mathbf{Q}_t \leftarrow \varepsilon_\theta(\tilde{\mathbf{Q}}_t; \mathbf{O}_t, \{1, \dots, f\})$                                  $\triangleright \varepsilon_\theta$  is trained using  $f$  noise levels
4:    $\mathbf{a}_t^{(0)} \leftarrow \mathbf{Q}_t.\text{pop}(0)$                                           $\triangleright \mathbf{a}_t^{(0)}$  is a clean action (fully denoised)
5:    $\tilde{\mathbf{Q}}_t \leftarrow \mathbf{Q}_t.\text{push}(\mathbf{z})$                                           $\triangleright \mathbf{z}$  is a random noisy action sampled from  $\mathcal{N}(\mathbf{0}, \mathbf{I})$ 
6:    $\mathbf{O}_t \leftarrow \text{env.step}(\mathbf{a}_t^{(0)})$                                           $\triangleright$  executes  $\mathbf{a}_t^{(0)}$  and environment updates observation
7:    $t \leftarrow t + 1$                                                $\triangleright$  update timestep for the next iteration

```

B.2 Noise-Relaying Diffusion Policy Training

We summarize the training pseudo-code of our RNR-DP in Algorithm 2.

Algorithm 2 Responsive Noise-Relaying Diffusion Policy Training

```

1: Require: demonstration dataset,  $\mathcal{D} = \{(\mathbf{O}_i, \mathbf{A}_i)\}_{i=1}^N$ ; denoising model,  $\varepsilon_\theta$ ; number of diffusion steps,  $f$ 
2: repeat
3:   Sample  $(\mathbf{O}, \mathbf{A}) \sim \mathcal{D}$ 
4:   Sample  $p \sim \text{Unif}(0, 1)$ ; Sample noise  $\epsilon \sim \mathcal{N}(0, \mathbf{I})$  and reshape to  $\mathbb{R}^{C_a \times f}$ 
5:   if  $p \leq p_{\text{linear}}$  :
6:      $\mathbf{k} = \{k_1 = 1, \dots, k_f = f\}$                                                $\triangleright$  linear schedule
7:   else
8:      $\mathbf{k} = \{k_1 \sim \text{Unif}(\{1, \dots, f\}), \dots, k_f \sim \text{Unif}(\{1, \dots, f\})\}$        $\triangleright$  random schedule
9:   for all  $\mathbf{a}_j \in \mathbf{A}$  indexed by frame index  $j$  do
10:     $\hat{\mathbf{a}}_j = \sqrt{\bar{\alpha}_{t_j}} \mathbf{a}_j + \sqrt{1 - \bar{\alpha}_{t_j}} \epsilon_j$             $\triangleright$  perturb each  $\mathbf{a}_j$  independently
11:     $\hat{\mathbf{A}} = \{\hat{\mathbf{a}}_0, \dots, \hat{\mathbf{a}}_{f-1}\}$ 
12:    Take gradient descent step to update  $\theta$  on
13:     $\nabla_\theta \|\epsilon - \varepsilon_\theta(\hat{\mathbf{A}}; \mathbf{O}, \mathbf{k})\|$                                       $\triangleright$  noise-aware conditioning
14: until converged

```

B.3 Policy Architecture

We build our RNR-DP on top of the UNet-based architecture of Diffusion Policy (Chi et al., 2023). The model includes 2 downsampling modules and 2 upsampling modules with each module containing 2 residual blocks. The residual block consists of 1D temporal convolutions (Conv1d), group normalizations (GN), and Mish activation layers. The encoded noise-aware conditioning data (Section 5.2) is fused into each residual block through the FiLM transformation (Perez et al., 2018). The raw conditioning data is of shape $R^{f \times (C_{\text{emb}} + C_{\text{state}})}$ for state policies and of shape $R^{f \times (C_{\text{emb}} + C_{\text{visual}} + C_{\text{state}})}$ for visual policies. See Figure 15 for the visualization of a visual policy. We follow the UNet denoiser design for the observation that transformer-based policies are more sensitive to hyperparameters and often require more tuning (Chi et al., 2023). The choice of policy architecture is orthogonal to our method and we believe our design would also improve this policy class.

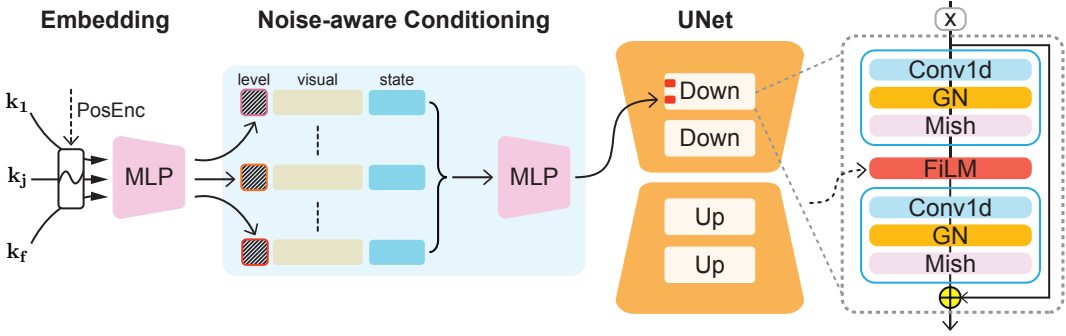


Figure 15: The detailed policy architecture for our RNR-DP. We only extract visual features for visual policies.

B.4 Important Hyperparameters

B.4.1 Key Hyperparameters of RNR-DP

We summarize the key hyperparameters of RNR-DP in Table 10. The observation horizon T_o and noise-relaying buffer capacity f for each task is listed in Table 11. The number of trainable parameters for each task is listed in Table 12.

Table 10: We list the key hyperparameters of RNR-DP used in our experiments.

Hyperparameter	Value
RNR-DP Noise Scheduling Scheme	Mixture Sampling(p_{linear}) $p_{\text{linear}} = 0.4$
RNR-DP Model Prediction Type	Noise
Diffusion Step Embedding Dimension	64
UNet Downsampling Dimensions	[64, 128, 256]
Optimizer	AdamW
Weight Decay	1e-6
Learning Rate	1e-4
Learning Rate Scheduler	Cosine
EMA Model Update	0.9999
Online Evaluation Episodes	1000

B.4.2 Key Hyperparameters of Diffusion Policy

We summarize the key hyperparameters of Diffusion Policy in Table 13. The observation horizon T_o , action execution horizon T_a and action prediction horizon T_p for each task are listed in Table 14.

B.5 Training Details

We train our models and baselines with cluster assigned GPUs (NVIDIA 2080Ti & A10). We use AdamW optimizer with an initial learning rate of 1e-4, applying 500 warmup steps followed by cosine decay. We use batch size of 1024 for state policies and 256 for visual policies for both ManiSkill and Adroit benchmarks. We evaluate DP, CP and RNR-DP model checkpoints using EMA weights every 10K training iterations for ManiSkill tasks and every 5K for Adroit tasks. DDIMs are evaluated using the best checkpoints of DDPMs in an offline manner. CPs are trained using the best checkpoints of EDMs.

Table 11: The observation horizon and noise-relaying buffer capacity of our RNR-DP for each task.

Task	Obs	T_o	Capacity f
ManiSkill3: PushT (Visual)	2	48	
ManiSkill3: RollBall (Visual)	2	64	
ManiSkill2: StackCube (Visual)	2	84	
Adroit: Pen (Visual)	2	4	
Adroit: Hammer (Visual)	2	64	
Adroit: Door (Visual)	2	56	
ManiSkill3: PushT (State)	2	32	
ManiSkill3: RollBall (State)	2	4	
ManiSkill2: StackCube (State)	2	84	
ManiSkill2: TurnFaucet w/g (State)	2	64	
ManiSkill2: TurnFaucet w/o g (State)	2	72	
ManiSkill2: PushChair w/g (State)	2	56	
ManiSkill2: PushChair w/o g (State)	2	48	
Adroit: Door (State)	2	74	
Adroit: Pen (State)	2	4	
Adroit: Hammer (State)	2	32	
Adroit: Relocate (State)	2	84	

Table 12: The number of our RNR-DP trainable parameters for each task. Noise-relaying buffer size doesn't affect the number of trainable parameters for each task.

Task	Trainable Params
ManiSkill3: PushT (Visual)	11.42M
ManiSkill3: RollBall (Visual)	11.59M
ManiSkill2: StackCube (Visual)	10.85M
Adroit: Pen (Visual)	14.67M
Adroit: Hammer (Visual)	14.72M
Adroit: Door (Visual)	14.41M
ManiSkill3: PushT (State)	4.53M
ManiSkill3: RollBall (State)	4.73M
ManiSkill2: StackCube (State)	4.91M
ManiSkill2: TurnFaucet (State)	4.71M
Adroit: Door (State)	4.66M
Adroit: Pen (State)	4.75M
Adroit: Hammer (State)	4.77M
Adroit: Relocate (State)	4.66M

C Additional Results

C.1 Empirical Comparison with Acceleration Methods on Visual Observations

We summarize the results of vision-based experiments in Table 15. As shown in Table 15, our RNR-DP outperforms all DDIM variations and CP variations and particularly has an overall improvement over 8-step DDIM by 6.9%, over 8-step-chaining CP by 3.4%.

Table 13: We list the key hyperparameters of Diffusion Policy baseline used in our experiments.

Hyperparameter	Value
Diffusion Step Embedding Dimension	64
UNet Downsampling Dimensions	[64, 128, 256]
Optimizer	AdamW
Weight Decay	1e-6
Learning Rate	1e-4
Learning Rate Scheduler	Cosine
EMA Model Update	0.9999
Online Evaluation Episodes	1000

Table 14: We list the observation horizon, action execution horizon and action prediction horizon of Diffusion Policy baseline for each task.

Task	Obs T_o	Act Exec T_a	Act Pred T_p
ManiSkill3: PushT (Visual)	2	2	16
ManiSkill3: RollBall (Visual)	2	4	16
ManiSkill2: StackCube (Visual)	2	8	16
Adroit: Pen (Visual)	2	8	16
Adroit: Hammer (Visual)	2	8	16
Adroit: Door (Visual)	2	8	16
ManiSkill3: PushT (State)	2	1	16
ManiSkill3: RollBall (State)	2	4	16
ManiSkill2: StackCube (State)	2	8	16
ManiSkill2: TurnFaucet (State)	2	8	16
Adroit: Door (State)	2	8	16
Adroit: Pen (State)	2	8	16
Adroit: Hammer (State)	2	8	16
Adroit: Relocate (State)	2	8	16

Table 15: Evaluation on simpler tasks (Regular Group) not requiring responsive control from ManiSkill and Adroit benchmarks (Visual Observations). We follow our evaluation metric and report values under the same settings as in Table 4. Tasks in which none of the methods achieve a reasonable success rate under visual observations are omitted.

Method	Steps (S)	NFEs/a	StackCube			Avg. SR of tasks
			Pen	Hammer		
DDPM	100	12.5	0.958	0.133	0.123	0.404
	1	0.125	0.000	0.000	0.000	0.000
	2	0.25	0.946	0.042	0.000	0.329
	4	0.5	0.947	0.125	0.000	0.357
	8	1	0.946	0.139	0.009	0.365
EDM	80	20	0.930	0.156	0.067	0.384
CP	1	0.125	0.615	0.127	0.088	0.277
	8	1	0.910	0.161	0.077	0.383
RNR-DP	1	1	0.924	0.154	0.110	0.396

C.2 Comparsion with Streaming Diffusion Policy (SDP)

Streaming Diffusion Policy (SDP) (Høeg et al., 2024) is a recent advancement over Diffusion Policy that stays close to our approach. In this section, we compare our method with SDP in terms of motivation (Appendix C.2.1), methodology (Appendix C.2.2), and empirical results (Appendix C.2.3).

C.2.1 Motivation Comparison

SDP accelerates Diffusion Policy inference by reducing the number of denoising steps required to generate an action sequence. While improving diffusion inference speed is a relevant research topic, its impact in robotics is less compelling, as DDIM and Consistency Policy already provide reasonable speedups with strong performance. In contrast, our method addresses a fundamental limitation of Diffusion Policy—its lack of responsiveness—which significantly hinders performance in rapidly changing environments (e.g., contact-rich dynamic object manipulation). This challenge is far more critical to advancing robotic control. Although our approach also serves as an effective acceleration method, we view this as a secondary benefit compared to its primary advantage of enabling more responsive control.

C.2.2 Method Comparison

Rollout Method SDP also employs an action buffer structure but partitions the prediction horizon T_p into multiple action chunks, ensuring that (1) each chunk maintains the same noise level and (2) noise levels increase across chunks. This chunk-wise design focuses solely on reducing denoising steps and accelerating inference. However, it does not address responsiveness and thus retains the limitations of Diffusion Policy. In contrast, our sequential denoising scheme conditions all actions on the latest observations, enabling responsive control while leveraging the noise-relaying buffer to maintain efficiency.

Policy Architecture SDP fuses all time embeddings along the temporal dimension into a single embedding. In contrast, our architecture retains multiple time embeddings, ensuring that noisy actions within the noise-relaying buffer can perceive time step changes based on the latest observation features. This design preserves temporal dynamics, allowing each action to adapt to varying time steps, thereby improving responsiveness and consistency in action generation.

C.2.3 Empirical Results Comparison

To demonstrate that SDP inherits the same limitations as Diffusion Policy and lacks responsive control, we conduct experiments on the Adroit Relocate task (see Table 16). As the empirical results indicate, Streaming Diffusion Policy performs similarly to Diffusion Policy on the Adroit Relocate task, whereas our method achieves significantly more responsive control than both.

Table 16: We compare Streaming Diffusion Policy with Diffusion Policy and our method on Adroit Relocate task.

Task	DP	SDP	RNR-DP
Relocate (Adroit)	0.422	0.436	0.585